

Energy Spectrum Characteristics of Boreal Summer Intraseasonal Oscillations: Climatology and Variations during the ENSO Developing and Decaying Phases*

AILAN LIN

Institute of Tropical and Marine Meteorology/Key Open Laboratory for Tropical Monsoon, China Meteorological Administration, Guangzhou, China

TIM LI

IPRC, and Department of Meteorology, University of Hawaii at Manoa, Honolulu, Hawaii

(Manuscript received 16 November 2007, in final form 16 April 2008)

ABSTRACT

The geographic-dependence characteristics of the energy spectrum of the boreal summer intraseasonal oscillation (BSISO; May–October) over the Indo–western Pacific region were analyzed using 25-yr (1979–2003) observational data. The BSISO energy spectrum distribution exhibits a distinctive regional characteristic. The stationary and eastward-propagating modes are most pronounced at the equator (5°S–5°N), while the westward-propagating modes are dominant in the off-equatorial region (10°–20°N). While the eastward intraseasonal oscillation (ISO) spectrum agglomerates on the 30–60-day period and zonal wavenumber 1, the westward mode covers wider spatial (wavenumber) and temporal (period) range. Along the Arabian Sea, Bay of Bengal, and South China Sea (SCS) latitudes, the dominant wavenumber 1 mode is the eastward (westward) propagation at the 30–60-day (10–20 day) period; for zonal wavenumber 2, the dominant mode is the westward propagation at both the 30–60-day and 10–20-day periods. Compared to the absolute amplitude of both zonal and meridional mode energy spectrum, northward propagation is the most predominant mode in boreal summer over the Indo–western Pacific regions. The strongest northward-propagating BSISO signal appears in the eastern tropical Indian Ocean.

The variation of BSISO differs significantly in the El Niño and La Niña developing and decaying phases. During the El Niño (La Niña) developing summer, the eastward propagation is enhanced (weakened) at the equator, while the northward propagation is also strengthened (weakened) over the western Pacific (east of 140°E). During the El Niño (La Niña) decaying summer, the eastward propagation weakens (strengthens) at the equator, opposite to that in the developing summer; the westward propagation off the equator and the northward propagation over SCS and the western Pacific are suppressed (enhanced). The amplitude of the BSISO variation is stronger in the decaying summer than that in the developing summer. This asymmetry in BSISO variations is primarily attributed to the asymmetry of the background mean flow change associated with the developing and decaying phases of ENSO.

1. Introduction

The intraseasonal oscillation (ISO) is one of dominant modes in tropical atmosphere. The evolution of the Asia monsoon system (e.g., its break and active phases) bears a notable ISO characteristic (Lau and

Yang 1996; Li and Li 1997; Li et al. 2001; Long and Li 2002; Li et al. 2003). For example, previous studies showed that floodwater-logging damage in East Asia (including heavy precipitation over middle–lower reaches of the Yangtze River and south China) links closely to ISO and its propagation (Shi and Ding 2000; Chen et al. 2001; Yang and Li 2003; Xu et al. 2004; Ju et al. 2005; Mao and Wu 2005; Han et al. 2006). The formation and track of tropical cyclones over the Indian and Pacific Oceans are also related to ISO to some extent (Lin et al. 2004; Zhu et al. 2004). Numerical weather prediction results showed that a model capable of simulating ISO may have a better overall forecast skill (Li et al. 2006).

ISO exhibits a pronounced seasonal variation. The

* School of Ocean and Earth Science and Technology Contribution Number 7480 and International Pacific Research Center Contribution Number 529.

Corresponding author address: Ailan Lin, Institute of Tropical and Marine Meteorology, China Meteorological Administration, Guangzhou 510080, China.
E-mail: allin@grmc.gov.cn

boreal summer ISO (BSISO) differs significantly from the boreal winter ISO in variance and propagation characteristics (Wang and Rui 1990, Madden and Julian 1994). While the boreal winter ISO is characterized by eastward propagation along the equator, BSISO exhibits a more complex propagation feature, including eastward propagation along the equator, northward propagation over the tropical Indian Ocean and western Pacific, and westward propagation off the equator (e.g., Yasunari 1979; Krishnamurti and Subrahmanyam 1982; Chen and Murakami 1988). The meridional propagation is dominated by northward propagation in boreal summer, even though weaker southward propagation is also observed along some longitudes (Yang and Li 2005). In addition to propagation components, ISO also has a stationary component (e.g., Zhu and Wang 1993).

The South China Sea (SCS) is a key region that connects the South Asian, East Asian, and western North Pacific (WNP) monsoons (Wang and LinHo 2002). The atmospheric ISO greatly affects the onset, evolution, and strength of the summer monsoon over SCS (e.g., Lin 1998; Li and Wu 2000; Shi and Ding 2000; Mu and Li 2000; Li et al. 2001; Li et al. 2003; Ju et al. 2005; Lin et al. 2006, 2007). ISO convective activities over SCS may originate from the equatorial region, western Pacific, Bay of Bengal, or in situ ocean (Waliser 1996; Zhang et al. 2002; Liang et al. 2005). The monsoon onset over SCS is often associated with the northward and/or westward propagation of ISO (Wang and Xu 1997; Zhang et al. 2002). The BSISO over SCS is closely related to the east–west displacement of the subtropical high over WNP (Lin 1998).

The modulation of the El Niño–Southern Oscillation (ENSO) on the boreal winter ISO has been studied in a great deal (e.g., Gutzler 1991; Fink and Speth 1997; Hendon et al. 1999; Kessler 2001). The general consensus is that the eastward-propagating ISO tends to strengthen (weaken) in the central Pacific during the warm (cold) episodes, and ISO activities over other regions are in general uncorrelated with ENSO. By applying a wavenumber–frequency spectral analysis in a regional (tropical Indian Ocean and western Pacific) domain, Teng and Wang (2003) quantified the relationship between the boreal summer ISO and ENSO. They found that both the westward- and northward-propagating ISOs are enhanced in late summer (July–October) when the eastern Pacific SST anomaly (SSTA) is simultaneously warm. The result is different from previous studies. The difference arises from the fact that most of the previous works studied the boreal winter MJO, while Teng and Wang (2003) dealt with boreal summer ISO. Because the atmospheric circulation changes dramatically during the developing and

decaying summers of ENSO, it is necessary to reveal the BSISO characteristics in the different phases of ENSO respectively. This motivates the current study.

The objective of the present work is to document the energy spectrum distribution and propagation characteristics of BSISO over the SCS and vicinity regions both in the climatology and during the developing and decaying phases of ENSO, and to further identify the possible mechanisms responsible for the asymmetric BSISO–ENSO relationships. The remainder of this paper is organized as follows. The data and methods used in this study are described in section 2. The energy spectrum distribution of BSISO as a function of wavenumber and frequency along different latitude and longitude bands is presented in section 3. The geographic dependence of the dominant BSISO mode at each region is described in section 4. The asymmetry of the BSISO–ENSO relationships during the developing and decaying phases of ENSO is investigated, and the possible mechanism for the relationships is discussed in section 5. Finally a summary is given in section 6.

2. Data and method

The primary datasets are 1979–2003 daily mean outgoing longwave radiation (OLR; Liebmann and Smith 1996), provided by the National Oceanic and Atmospheric Administration (NOAA)–Cooperative Institute for Research in Environmental Sciences (CIRES) Climate Diagnostics Center, and the monthly National Centers for Environmental Prediction/Department of Energy (NCEP–DOE) Reanalysis 2 (Kanamitsu et al. 2002). These datasets have a $2.5^\circ \times 2.5^\circ$ global coverage. The additional dataset is monthly sea surface temperature (SST) at a $1^\circ \times 1^\circ$ resolution from Global Sea Ice and Sea Surface Temperature Data (GISST) compiled by the Hadley Centre for Climate Prediction and Research, Met Office (Rayner et al. 1996).

A wavenumber–frequency analysis is employed to transform the OLR field from a spatial–time domain to a wavenumber–frequency domain. Conventionally, a spatial decomposition is carried out along a full longitude circle (e.g., Hayashi 1982; Chen et al. 2000). Following Teng and Wang (2003), we extend the wavenumber–frequency analysis from a global domain to a finite domain (10°S – 30°N , 40°E – 180°), as BSISO convection is effectively trapped in the summer monsoon region by the lower boundary conditions (such as SST and land and ocean surface moisture distribution; Li and Wang 1994) and the three-dimensional background monsoon flows (Wang and Xie 1997). The ISO in the present study is defined at a period of 10–90 days. Because our focus is on BSISO, all spectrum analysis is

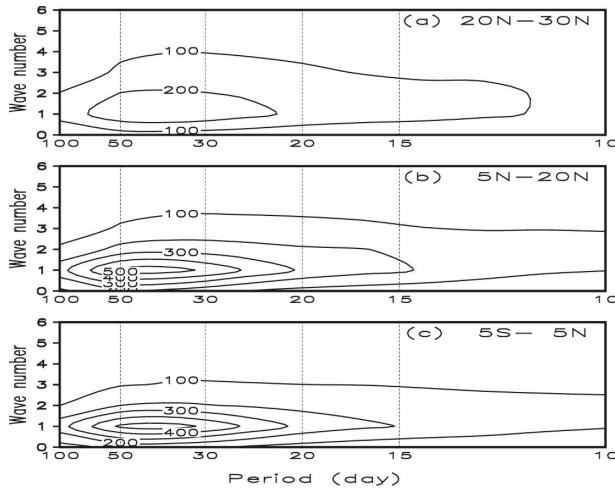


FIG. 1. Climatological energy spectrum distribution of the zonal BSISO (May–October) mode during 1979–2003 along (a) 20°–30°N, (b) 5°–20°N, and (c) 5°S–5°N as a function of wavenumber and period for OLR anomalies at 40°E–180°.

conducted for the period from May to October each year. To minimize the effect of discontinuity in the OLR time series, our strategy is to calculate the spectrum at each summer (May–October) first and then conduct an averaging for the 25-yr spectrum. By doing so one does not need to tamper the time series at either end. For the limited domain analysis, zonal wavenumber 1 corresponds to a wavelength of 140° in longitude, and meridional wavenumber 1 corresponds to a wavelength of 40° in latitude. The annual mean and the first four harmonics are removed from original time series before the wavenumber–frequency analysis is performed.

Two-sample Student's t tests are applied to test the significance of difference between El Niño and La Niña composites.

3. Climatological BSISO energy distribution in a wavenumber–frequency domain

As the BSISO convection is primarily restricted to the Asian monsoon region, a finite domain of 10°S–30°N, 40°E–180° is chosen for the OLR wavenumber–frequency analysis (May–October). Figure 1 illustrates climatological mean energy spectrum for 1979–2003 as a function of wavenumber and period for zonal (propagating and stationary) modes at three latitude bands. At each band, the strongest energy power resides on the period of 30–60 days and zonal wavenumber 1 (which corresponds to a wavelength of 140° in longitude). For the wavenumber 1 and the 30–60-day period the highest energy spectrum (with a value of about 500

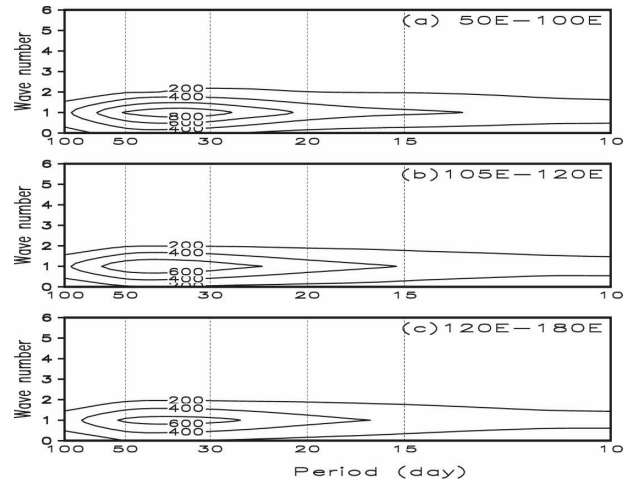


FIG. 2. Climatological energy spectrum distribution of the meridional BSISO (May–October) mode during 1979–2003 along (a) 50°–100°E, (b) 105°–120°E, and (c) 120°E–180°E as a function of wavenumber and period for OLR anomalies at 10°S–30°N.

$\text{W}^2 \text{m}^{-4}$) appears at the equatorial (5°S–5°N) and the Arabian Sea (AS), Bay of Bengal (BOB), and SCS (hereafter, ABS) latitudinal (5°–20°N) bands. The energy spectrum decreases sharply with the increasing of zonal wavenumber. For example, the energy of wavenumber 2 (wavenumber 4) is about half (one fifth) of that of wavenumber 1. On the 10–20-day period, the energy is weaker than that of the 30–60-day period, and the difference between wavenumber 1 and wavenumber 2 becomes less. The BSISO energy along the Asian continent latitudinal band (20°–30°N) is much weaker than that to the south. A further separation of the zonally propagating and the nonpropagating (stationary) ISO modes shows that, while the energy distribution patterns of the two modes are similar, the amplitude of the propagating mode is much greater than the stationary mode (figures not shown).

To test the sensitivity of the regional spectrum analysis to longitudinal domain, we performed additional analyses by extend the zonal domain to 180° (i.e., 20°E–160°W) and 360°. It is noted that wavenumber 1 spectrum is still dominant in the 180° domain. The dominant modes become wavenumber 1 and 2 when a 360° global domain is used. The result is consistent with the works of Hendon and Salby (1994). It is also noted that the spectrum amplitudes in the extended zonal domain cases are weaker than that in Fig. 1, implying that BSISO convection is effectively trapped in the Eastern Hemisphere and Asian summer monsoon region.

To examine the energy distribution of the BSISO meridional mode, the finite domain wavenumber–frequency analysis is performed over 10°S–30°N. Figure 2

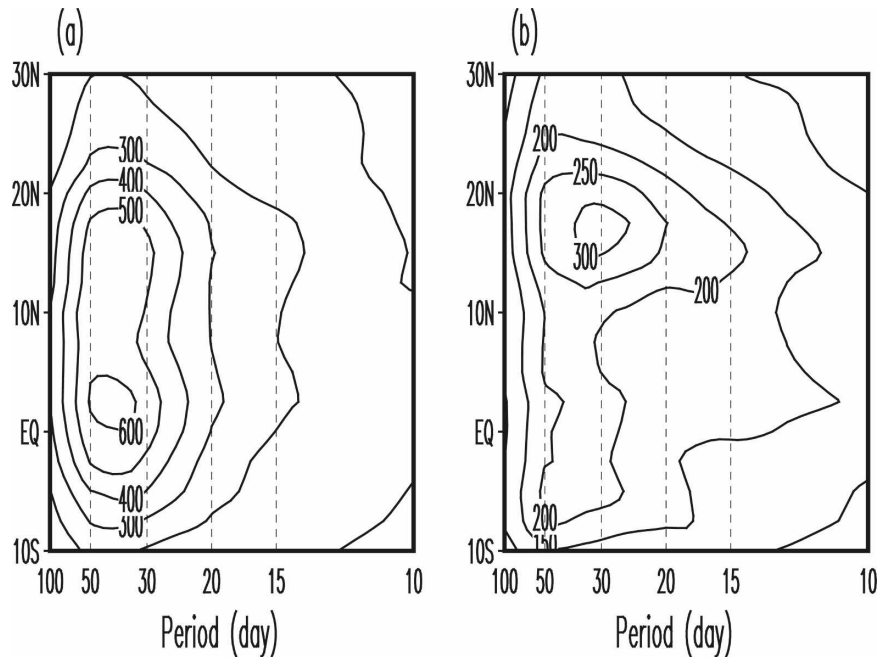


FIG. 3. BSISO (May–October) energy spectrum as a function of lat and period for zonal wavenumber (a) 1 and (b) 2.

shows that the strongest energy spectrum appears on the period of 30–60 days at meridional wavenumber 1 (corresponding to a wavelength of 40° in latitude). Comparing the spectrum distribution along three longitudinal bands over the Indian Ocean (50° – 100° E; Fig. 2a), SCS (105° – 120° E; Fig. 2b), and western Pacific (120° E– 180° ; Fig. 2c), one finds that the meridional ISO mode is the strongest over the Indian Ocean, followed by that over SCS and the western Pacific. The northward-propagating ISO mode has similar energy distribution to Fig. 2, and its amplitude is stronger than the combined southward-propagating and stationary modes over the Indian Ocean and SCS (figures not shown).

Thus, for both the propagating and stationary modes, the strongest energy spectrum appears on the period of 30–60 days and at wavenumber 1 in either meridional or zonal direction over the Indo–western Pacific region (10° S– 30° N, 40° E– 180°). Zonal ISO modes retain strong power along the equatorial and ABS latitudes, and less power over the Asian continent band (north of 20° N). Meridional ISO modes over the Indian Ocean (50° – 100° E) are the strongest.

4. Geographic dependence of the climatological BSISO spectrum

In this section we examine the geographic dependence of the dominant BSISO modes. Given that the

strongest BSISO energy is confined in the lowest wavenumbers, here we focus on the zonal or meridional wavenumber 1 and wavenumber 2 modes.

a. Zonally propagating/stationary modes

Figure 3 shows the ISO spectrum (including both the zonally propagating and stationary modes) as a function of latitude and period. Note that for the zonal wavenumber 1 (Fig. 3a), the BSISO has the maximum energy spectrum at the equatorial (0° – 5° N) and the ABS (5° – 20° N) latitudes and decays rapidly in the Asian continent (20° – 30° N) band. The ISO strength at 20° – 30° N is only about a half of that at the equator. In contrast, for the wavenumber 2 (Fig. 3b), the strongest ISO spectrum locates off the equator (10° – 20° N) with a broader period (20–60 days).

By separating the propagating mode from the stationary mode, one finds that the zonal wavenumber 1 propagating ISO retains two maximum centers in the ABS and the equatorial latitudes, and decays rapidly in the higher latitudes (20° – 30° N; Fig. 4a). This latitudinal distribution differs from that of the stationary mode, which shows a single maximum center right on the equator. Thus the difference in the total ISO spectrum between the equatorial and ABS latitudinal band is attributed to that of the stationary mode. In contrast to the zonal wavenumber 1, both the stationary and the propagating modes at the zonal wavenumber 2 have

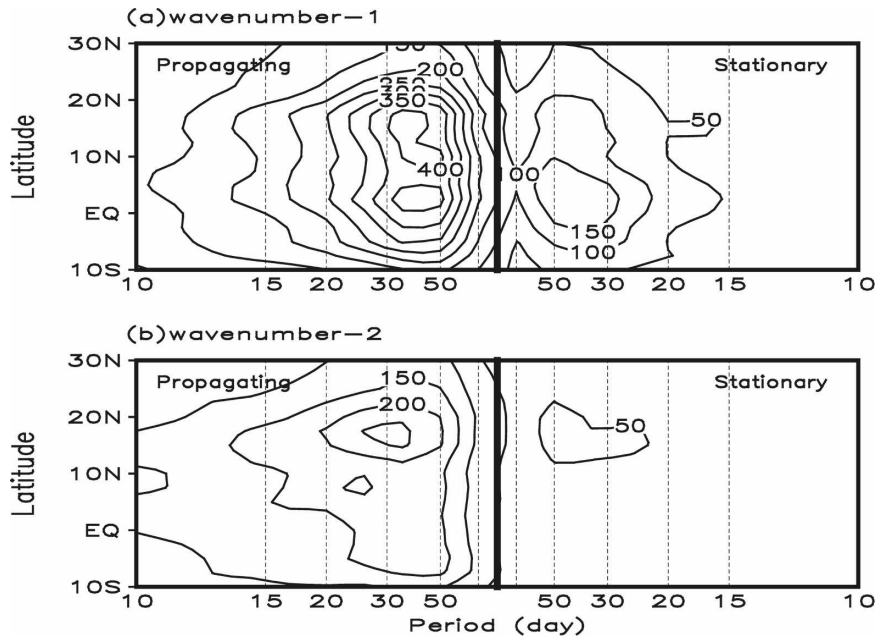


FIG. 4. Energy spectrum of the (left) zonal-propagating and (right) stationary BSISO (May–October) modes during 1979–2003 as a function of lat and period for zonal wavenumber (a) 1 and (b) 2.

maximum spectrum off the equator (Fig. 4b). The amplitude of the propagating mode is always stronger than the stationary mode, indicating a dominant propagating characteristic for BSISO.

The zonally propagating mode consists of both eastward and westward propagation. It is shown from Fig. 5 that the eastward propagation is most pronounced at the equator, whereas the westward propagation is strongest off the equator (10° – 20° N), for both the zonal wavenumber 1 and wavenumber 2. The dominant period for the eastward propagation is confined to 30–60 days, while the dominant period of the westward propagation is wider, covering both the biweekly (10–20 day) and longer periods. Furthermore, for the zonal wavenumber 1, the energy of the eastward propagation is greater than that of the westward propagation. This is different from the zonal wavenumber 2 in which the westward-propagating mode retains greater energy. The result implies that higher wavenumber contribution needs be considered for the westward-propagating ISO. The westward energy is of comparable amplitude for wavenumber 1 and 2.

The fact that in the 30–60-day band there is more power in the eastward- than westward-propagating components is consistent with many previous studies (e.g., Madden and Julian 1971; Lau and Chan 1986; Salby and Hendon 1994; Wheeler and Kiladis 1999; Teng and Wang 2003).

The dependence of energy spectrum of various

BSISO modes on zonal wavenumber is shown in Fig. 6. The 30–60-day eastward-propagating mode on the equator (5° S– 5° N) retains the highest energy power at wavenumber 1 and weakens sharply with increased wavenumber (dash line). For example, the energy on the wavenumber 2 and wavenumber 3 accounts for only 37% and 13% of that on the wavenumber 1. The energy of the eastward propagation at the period of 10–20 days (thick bar) is weaker than that of the 30–60-day period, especially on the wavenumber 1. Thus, the eastward-propagating ISO concentrates most of its energy on the wavenumber 1 and the 30–60-day period. The energy of the 30–60-day westward-propagating mode off the equator (10° – 20° N) decreases with the increased wavenumber at a much slower rate (Fig. 6, solid line). For example, the energy on the wavenumber 2 and wavenumber 3 attains 67% and 35% of that on the wavenumber 1. For the 10–20-day period, the westward propagation retains the strongest power on wavenumber 2.

To examine the relative contribution of eastward, westward, and stationary modes, we introduce absolute and relative energy contribution percentage concepts. The absolute contribution percentage measures the ratio of the spectrum of an individual mode (say, eastward, westward, or stationary mode) to the total ISO spectrum. The relative contribution percentage is a ratio between the eastward and the westward propagation spectrum. A relative contribution value of greater

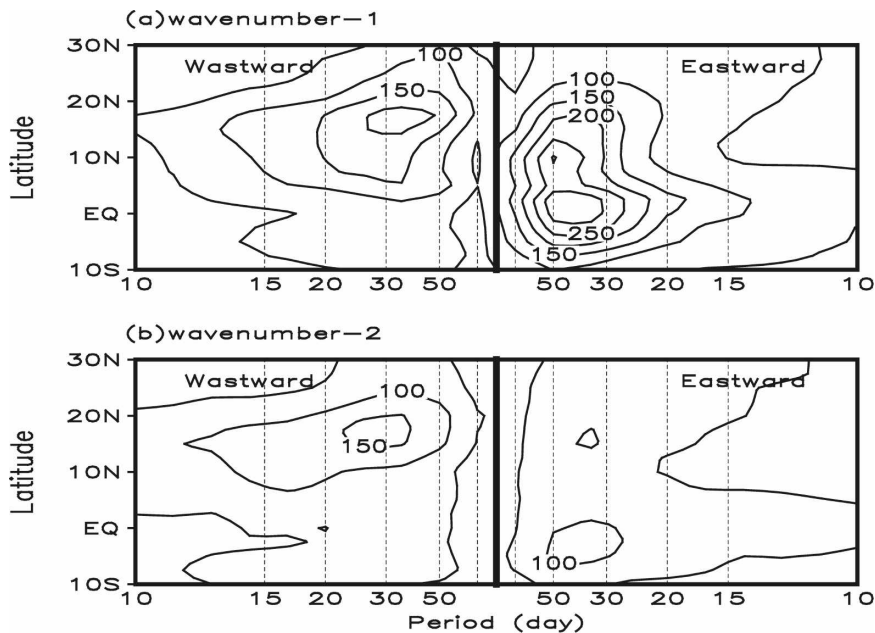


FIG. 5. (left) Westward- and (right) eastward-propagating BSISO (May–October) spectrum during 1979–2003 as a function of lat and period for zonal wavenumber (a) 1 and (b) 2.

(less) than one indicates that the eastward (westward) propagating mode is stronger. Figure 7 illustrates the latitudinal dependence of the relative contribution percentage for the periods of 30–60 days and 10–20 days at the zonal wavenumber 1 and wavenumber 2. For the 30–60-day wavenumber 1 mode, the eastward propagation is stronger than the westward propagation at 10°S–15°N (Fig. 7a, solid line). Especially near the equator, the power of the eastward propagation is 4 times as large as that of the westward propagation. The westward propagation is stronger than the eastward propagation at 15°–30°N. For the biweekly mode (Fig. 7a, dash line), the westward propagation is about twice as strong as the eastward propagation over the ABS latitudes (10°–20°N), while the eastward propagation is stronger on the equator and in the higher latitudes. The relative energy contribution percentage for the zonal wavenumber 2 (Fig. 7b) bears a similar latitudinal distribution as the wavenumber 1, except that the relative strength of the westward propagation increases.

b. Meridional modes

The meridional BSISO modes are pronounced in the eastern Indian Ocean, SCS, and western Pacific regions (Fig. 8). A minimum spectrum gap appears in the Sumatra and western Indochina peninsular longitudes (95°–105°E). The spectrum minimum over the Indochina peninsular region implies that air–sea interactions or wind-induced heat exchange may be important

for maintaining the intraseasonal variability. The meridional wavenumber 2 spectrum is much weaker than that of the wavenumber 1, even though their distribution patterns look similar.

Compared to the spectrum of the meridional propagating modes, the stationary modes retain much less energy (Fig. 9). The distribution pattern of both the propagating and stationary modes, however, bears

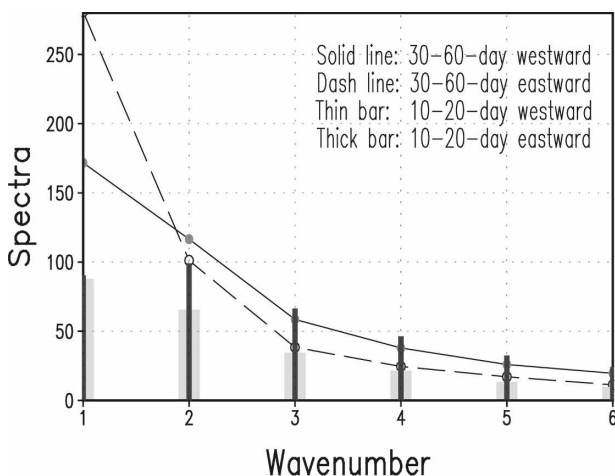


FIG. 6. Dependence on zonal wavenumber of the energy spectrum of the 30–60-day (dash line) and 10–20-day (thick bar) eastward-propagating modes averaged over the equatorial region (5°S–5°N) and the 30–60-day (solid line) and 10–20-day (thin bar) westward-propagating modes averaged over 10°–20°N.

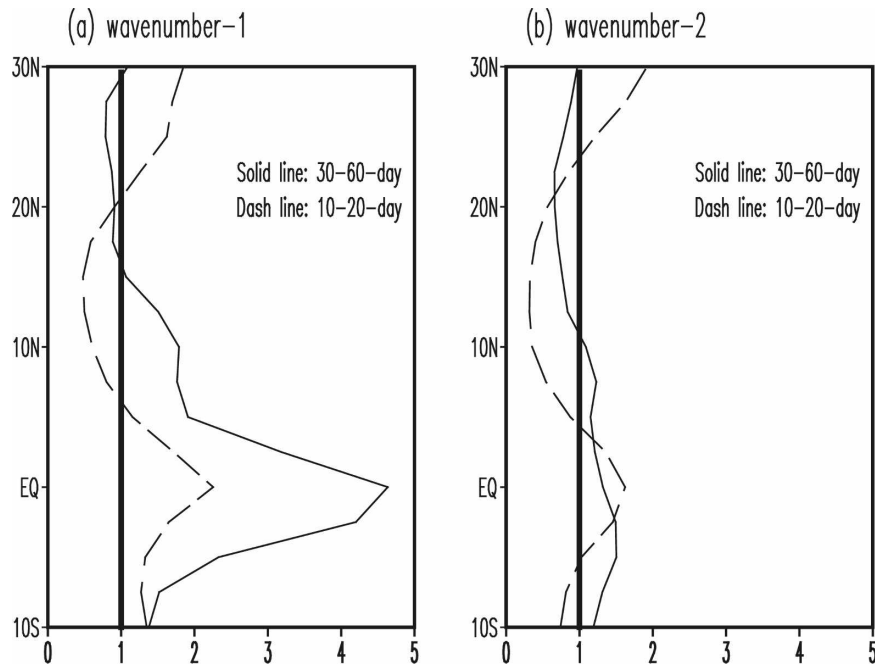


FIG. 7. The latitudinal distribution of the relative energy contribution percentage at the period of 30–60 days (solid line) and 10–20 days (dash line) for zonal wavenumber (a) 1 and (b) 2.

many similarities. A further separation of spectrum of northward and southward propagation shows that the northward-propagating mode is about 3 times (2 times) greater than the southward-propagating mode over the Indian Ocean (SCS and the western Pacific). The result agrees with the previous studies (e.g., Lau and Chan 1986; Jiang et al. 2004; Fu and Wang 2004). The strongest northward-propagating BSISO signal appears in the eastern tropical Indian Ocean, with a dominant period of 20–50 days (Fig. 10).

c. Dominant BSISO modes in different regions

Table 1 lists the energy spectrum and absolute energy contribution percentage of individual ISO modes (i.e., eastward, westward, and stationary modes) at different latitudinal (equator, ABS, and Asian continent) bands for the zonal wavenumber 1. The values outside (inside) a bracket correspond to the energy or the absolute energy contribution percentage with the period of 30–60 (10–20) days. Table 2 is the same as Table 1 except for the zonal wavenumber 2. It is demonstrated from Table 1 and Table 2 that the energy spectrum on the 30–60-day period is always greater than that on the 10–20-day period in all three regions. If defining the mode with the highest absolute energy contribution percentage as the dominant mode (marked with * in the tables) in a particular latitudinal band, one finds that

different regions possess different dominant modes. For example, along the ABS latitudinal (5° – 20° N) band, the dominant mode at the 30–60-day period and zonal wavenumber 1 is eastward propagation, while the dominant mode with the same zonal wavenumber at the 10–20-day period is westward propagation. The dominant mode at the zonal wavenumber 2 is westward propagation for both the 30–60-day and 10–20-day pe-

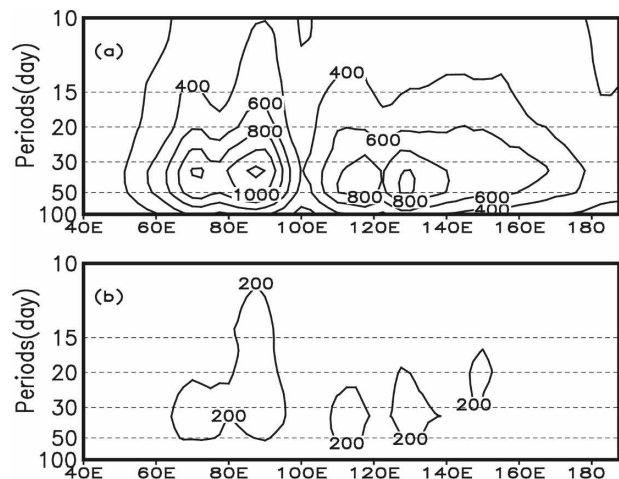


FIG. 8. Energy spectrum of the meridional BSISO (May–October) mode during 1979–2003 as a function of lon and period for meridional wavenumber (a) 1 and (b) 2.

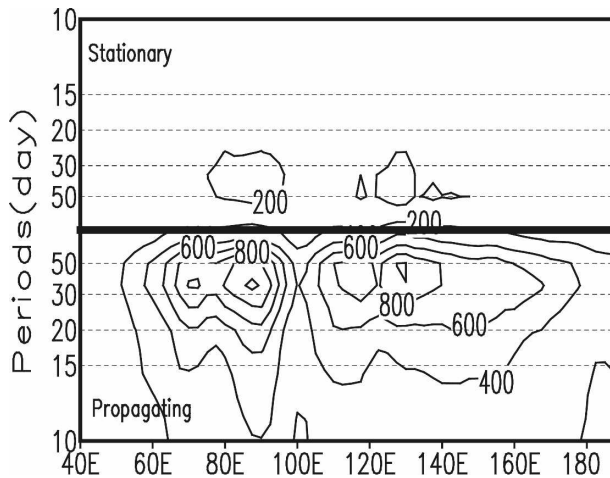


FIG. 9. The wavenumber 1 (bottom) propagating and (top) stationary components of energy spectrum of the meridional BSISO (May–October) modes during 1979–2003 as a function of lon and period.

riods. Over the equator (5°S – 5°N), the dominant mode is eastward propagation for zonal wavenumber 1 and wavenumber 2 at both the 30–60-day and 10–20-day periods. In the higher latitudes (20° – 30°N), the dominant mode propagates westward (eastward) at the period of 30–60 days (10–20 days). It is concluded that the BSISO favors eastward propagation along the equator for all wavenumbers and periods, while in the ABS and higher latitudes the dominant mode varies with the spatial scale and/or period.

Tables 3 and 4 show the spectrum and the absolute energy contribution percentage for different meridional modes. Note that the northward propagation is the dominant mode along all three longitudinal bands (over the tropical Indian Ocean, SCS, and western Pacific) for all meridional wavenumbers and periods. The most of BSISO energy is confined to the wavenumber 1; as a result the energy on the wavenumber 2 is only about 20% of that on the wavenumber 1. A further comparison of Tables 1 and 3 points out that the energy spectrum of the northward propagation is much greater than that of any individual zonal modes. The sum of the

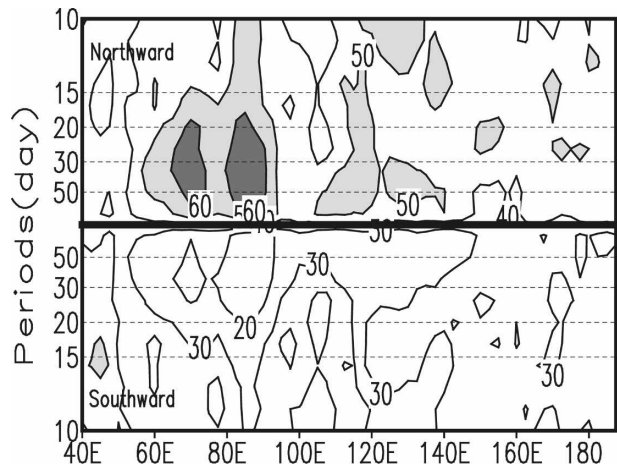


FIG. 10. Absolute energy contribution percentage of the wavenumber 1 (top) northward- and (bottom) southward-propagating BSISO (May–October) during 1979–2003 as a function of lon and period. The shading area indicates the energy percentage exceeding 50%.

first four wavenumber spectrums for both the zonal and meridional modes shows the same conclusion. Therefore, the northward-propagating ISO is the most predominant mode in the tropical Indian Ocean–western Pacific region in boreal summer.

5. Relationships between BSISO and ENSO

Many of previous studies focused on the boreal winter ISO–ENSO relationship (e.g., Gutzler 1991; Fink and Speth 1997; Hendon et al. 1999; Kessler 2001). Teng and Wang (2003) studied the simultaneous relationship between the boreal summer ISO and the eastern Pacific SSTA. This simultaneous relationship, however, is crude and sometimes misleading, because the atmospheric circulation is distinctively different between the ENSO developing and decaying summer. Thus in order to understand the true nature of interannual variability of the BSISO, it is necessary to examine the BSISO energy spectrum characteristics separately during the developing and decaying phases of ENSO.

The composite difference of BSISO strength (repre-

TABLE 1. The energy spectrum and absolute energy contribution percentage of the zonal wavenumber 1 modes at the period of 30–60 days and 10–20 days. The values outside (inside) brackets are the energy or energy percentage of the 30–60-day (10–20 day) period. The values marked with * denote the dominant mode in each lat band.

Region/mode	Stationary		Eastward		Westward	
	Spectrum	Percentage	Spectrum	Percentage	Spectrum	Percentage
Equator (5°S – 5°N)	164 (38)	30 (21)	281 (88)	52* (48*)	88 (52)	18 (31)
ABS (5° – 20°N)	134 (34)	25 (19)	229 (58)	43* (33)	161 (87)	32 (48*)
Asia continent (20° – 30°N)	69 (25)	24 (20)	98 (57)	36 (47*)	121 (42)	40* (33)

TABLE 2. The energy spectrum and absolute energy contribution percentage of the zonal wavenumber 2 modes at the period of 30–60 days and 10–20 days. The values outside (inside) brackets are the energy or energy percentage of the 30–60-day (10–20 day) period. The values marked with * denote the dominant mode in each latitudinal band.

Region/mode	Stationary		Eastward		Westward	
	Spectrum	Percentage	Spectrum	Percentage	Spectrum	Percentage
Equator (5°S–5°N)	39 (30)	18 (20)	101 (66)	47* (44*)	67 (53)	35 (36)
ABS (5°–20°N)	48 (32)	20 (19)	92 (41)	38 (26)	104 (93)	42* (55*)
Asia continent (20°–30°N)	41 (23)	20 (19)	70 (49)	35 (43*)	94 (46)	45* (38)

sented by the standard deviation of the filtered OLR time series) between El Niño and La Niña developing summers (Fig. 11a) shows that the most significant difference appears in the equatorial western Pacific (140°E–180°) and the equatorial western Indian Ocean (40°–60°E). Here El Niño (La Niña) developing summer is defined as the summer immediately before the peak phase of an El Niño (La Niña) event and El Niño (La Niña) decaying summer is defined as the summer immediately after the peak phase of an El Niño (La Niña) event. Note that the BSISO strength is enhanced (suppressed) in both the aforementioned regions during the developing year of El Niño (La Niña). However, a more significant change of the BSISO strength occurs during the decaying summer of ENSO over the SCS and vicinity regions. Figure 11b shows that the BSISO intensity weakens (strengthens) distinctly in the El Niño (La Niña) decaying summer over the large portion of the northern Indian Ocean, SCS, and WNP. The result above indicates that the variation of the BSISO is asymmetric between the ENSO developing and decaying summer, this is, the variation is much stronger in the El Niño–La Niña decaying summer than in the developing summer, even though the composite eastern equatorial SSTA is much weaker in the decaying summer.

Even for the same developing or decaying phase, there might be an asymmetry between the El Niño and La Niña. The cause of the asymmetry is possibly attributed to the amplitude difference of the SSTA between the warm and cold episodes. Even given the same SSTA pattern with an opposite sign, atmospheric non-

linearities may cause the different wind response (Kang and Kug 2002). To illustrate the asymmetry, we examine the BSISO spectrum anomaly (by subtracting its climatological mean value) at the El Niño and La Niña developing phases (Figs. 12a,b). Here we focus on the zonal wavenumber 1 BSISO spectrum (as a function of latitude and period). The change of the eastward-propagating BSISO spectrum appears larger during El Niño than during La Niña, whereas the change of the westward-propagating BSISO spectrum is larger during La Niña. From the El Niño–La Niña difference field (Fig. 12c), one finds that the most significant change is the enhancement (suppression) of eastward propagation at the equator (5°S–5°N) and westward propagation off the equator (5°–10°N) during the El Niño (La Niña) developing summer. No significant zonal-propagating BSISO variations occur along the ABS and higher latitudinal bands. The stationary mode at 5°S–10°N is strengthened (weakened) during the El Niño (La Niña) developing summer (figure not shown).

The change of the northward-propagating BSISO spectrum also exhibits an asymmetry between the El Niño and La Niña (Fig. 13). The northward propagation is enhanced (suppressed) over the western Pacific (east of 140°E) during the developing summer of El Niño (La Niña), and the amplitude of the change during the El Niño is twice as large as that during the La Niña. Over the SCS region (105°–120°E), the northward propagation behaves differently for different periods—it is strengthened (weakened) at the 30–60-day period but weakened (strengthened) at the 12–20-day period during the El Niño (La Niña). This frequency-

TABLE 3. The energy spectrum and absolute energy contribution percentage of the meridional wavenumber 1 modes at the period of 30–60 days and 10–20 days. The values outside (inside) brackets are the energy or energy percentage of the 30–60-day (10–20 day) period. The values marked with * denote the dominant mode in the longitudinal band of the eastern Indian Ocean (EIO), SCS, and western Pacific (WP).

Region/mode	Stationary		Northward		Southward	
	Spectrum	Percentage	Spectrum	Percentage	Spectrum	Percentage
EIO (60°–95°E)	198 (72)	22 (19)	542 (198)	59* (49*)	149 (113)	19 (32)
SCS (105°–120°E)	176 (77)	22 (20)	414 (184)	52* (45*)	187 (132)	26 (35)
WP (120°–140°E)	206 (82)	23 (21)	472 (196)	51* (49*)	207 (113)	26 (30)

TABLE 4. The energy spectrum and absolute energy contribution percentage of the meridional wavenumber 2 modes at the period of 30–60 days and 10–20 days. The values outside (inside) brackets are the energy or energy percentage of the 30–60-day (10–20 day) period. The values marked with * denote the dominant mode at EIO, SCS, and WP.

Region/mode	Stationary		Northward		Southward	
	Spectrum	Percentage	Spectrum	Percentage	Spectrum	Percentage
EIO (60°–95°E)	45 (35)	22 (20)	92 (75)	44* (45*)	70 (57)	34 (35)
SCS (105°–120°E)	44 (29)	22 (20)	88 (63)	44* (45*)	68 (48)	34 (35)
WP (120°–140°E)	43 (30)	22 (20)	81 (69)	41* (46*)	71 (50)	37 (34)

dependent feature also appears for the stationary and southward modes.

During the decaying summer of El Niño (La Niña), the eastward-propagating ISO mode is suppressed (strengthened) along the equator (Fig. 14). This is opposite to that in the developing summer. The westward propagation over the latitudinal band of 10°–18°N and the northward propagation over the longitudinal bands of 100°–120°E and 150°–170°E are significantly suppressed (enhanced) during the decaying summer of El Niño (La Niña). Thus, both the westward- and northward-propagating BSISO modes over the SCS region have a consistent response to ENSO in the decaying phase. The stationary mode over SCS, on the other hand, has little change. The fact that the westward and northward modes over SCS have more significant variations in the ENSO decaying summer than in the developing summer suggests that the east Pacific SSTA may exert a lagged impact on BSISO in the region. This may provide a precursor signal for BSISO forecast over the SCS region.

The analysis above clearly indicates that the interannual variation of BSISO depends on the phases of El Niño (La Niña). In the developing summer of El Niño (La Niña), both the eastward-propagating and stationary modes are strengthened (suppressed) on the equator; over the SCS longitudes (105°–120°E), the northward propagation with the period of 30–60 days is suppressed (enhanced) but it is opposite for the 12–20-day period. In the decaying summer of El Niño (La Niña), the equatorial eastward-propagating mode is suppressed (strengthened); so are the westward mode off the equator and the northward mode over SCS and western Pacific. It is demonstrated that the change of BSISO is more significant in the decaying summer than in the developing summer. The spectrum change of the eastward, westward (along 5°–20°N), and northward (along 105°–120°E) mode between El Niño and La Niña during the decaying phase accounts for 20%, 36%, and 61% of their climatological mean values.

The physical mechanism responsible for the asymmetry between the ENSO developing and decaying phases is discussed below. First, we focus on the asymmetry in

the eastward propagation at the equator. Under the normal (non-ENSO) condition, convection is suppressed in the central and eastern Pacific because of the cold tongue and the subsidence branch of the Walker circulation there. Therefore, an equatorial coupled Kelvin–Rossby wave ISO packet collapses after it reaches the date line. Rossby waves emanated from the decaying wave packet are reorganized and propagate westward under the WNP monsoon environment (Wang and Xie 1997). Figure 15 illustrates the zonal wind distribution at 850 hPa in the summer of El Niño and La Niña developing year and their difference. During the developing phase of El Niño, the westerly expands eastward to the east of 160°E, so is the location of large-scale convection as inferred from the OLR field (Fig. 16a). Under this condition, the equatorial coupled Kelvin–Rossby wave packet can reach to the easternmost location, thus enhancing the overall intensity of the eastward-propagating ISO. The condition is reverse in the developing phase of La Niña. In the decaying summer of El Niño, a low-level anticyclone anomaly appears over the Philippine Sea (Wang et al. 2000). This leads to easterly wind anomalies and the suppression of convection in the western Pacific (Figs. 17a,b). As a result, the coupled Kelvin–Rossby wave packet collapses at the westernmost location, which reduces the power of the eastward-propagating mode.

The possible mechanism for the asymmetry in the northward propagation is discussed below. As indicated by Jiang et al. (2004), the vertical shear of the mean flow and the meridional distribution of moist static energy may cause the northward propagation of BSISO. During the El Niño developing summer, the equatorial ISO packets propagates further to the east, which causes more Rossby wave emanation to the east of 140°E. Meanwhile, the enhanced vertical easterly shear (Fig. 16b) and low-level cyclonic vorticity (Fig. 16c) in the WNP favor the growth of Rossby waves and thus the northward- and westward-propagating ISO modes to the east of 140°E. As the biweekly mode over SCS is originated in the WNP, the favorable background condition also enhances the 10–20-day mode over the SCS region. In the decaying summer of El Niño, the Philip-

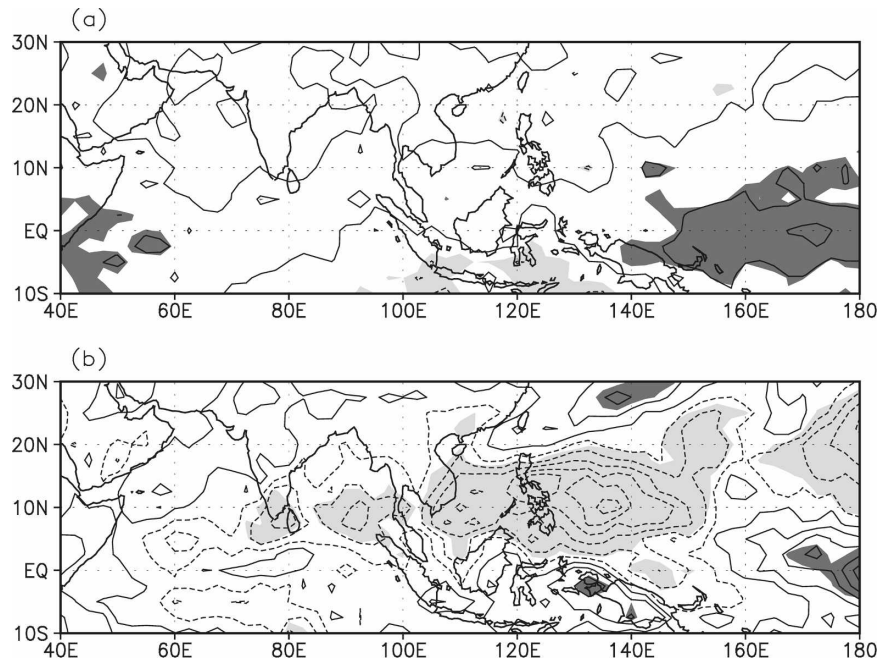


FIG. 11. Composite difference of the BSISO intensity [represented by the std dev of the filtered OLR time series (Wm^{-2})] between El Niño and La Niña (a) developing summer and (b) decaying summer. Shading indicates the 95% confidence level (CL).

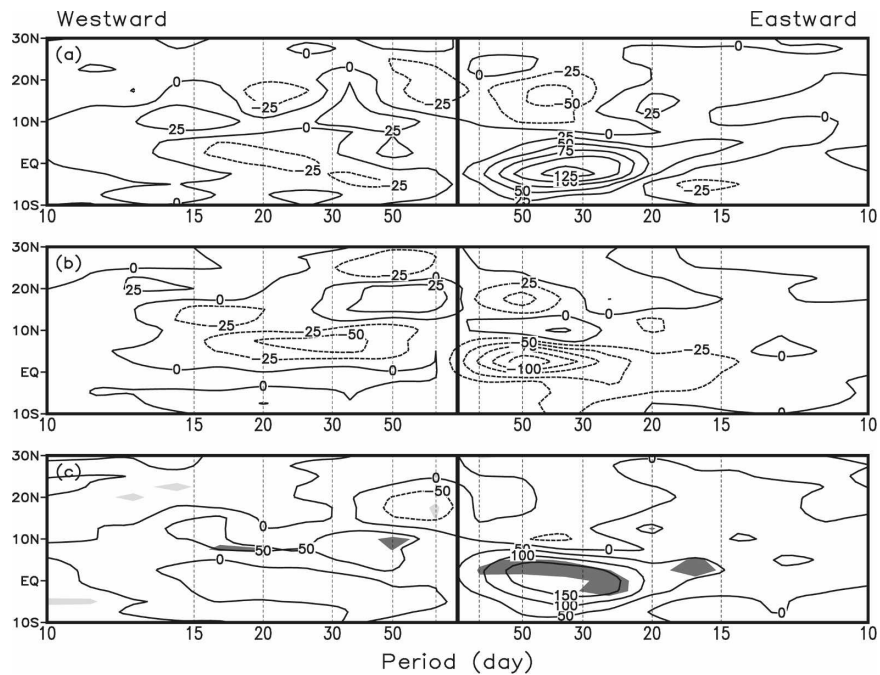


FIG. 12. Anomalous energy spectrum (by subtracting the climatological mean spectrum) of the zonal wavenumber 1 (left) westward- and (right) eastward-propagating BSISO during the (a) El Niño developing summer and (b) La Niña developing summer and (c) their difference. Shading in (c) denotes the 95% significance level.

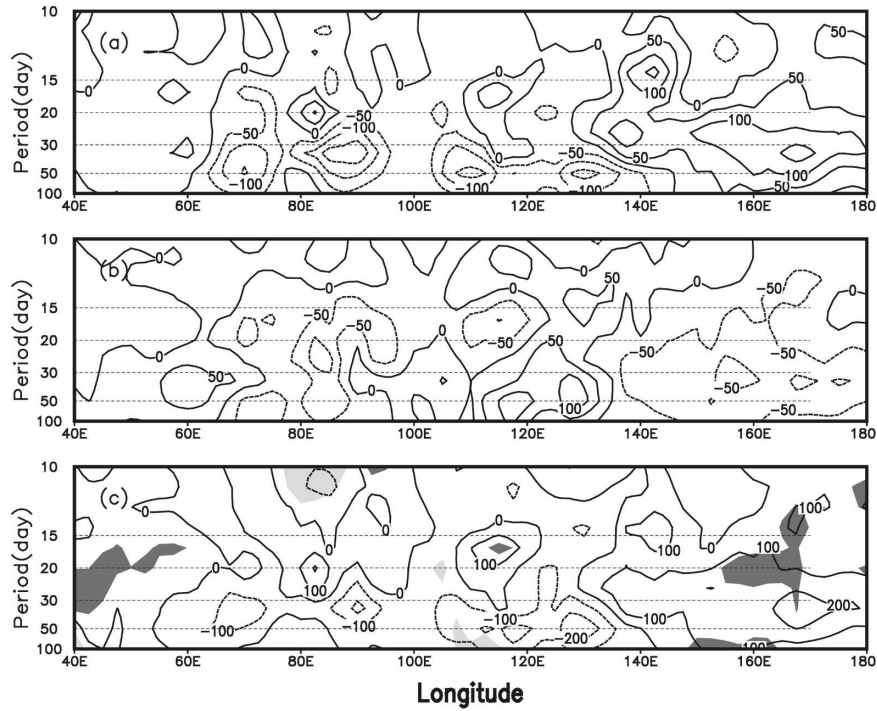


FIG. 13. Same as Fig. 12 but for the wavenumber 1 northward-propagating mode.

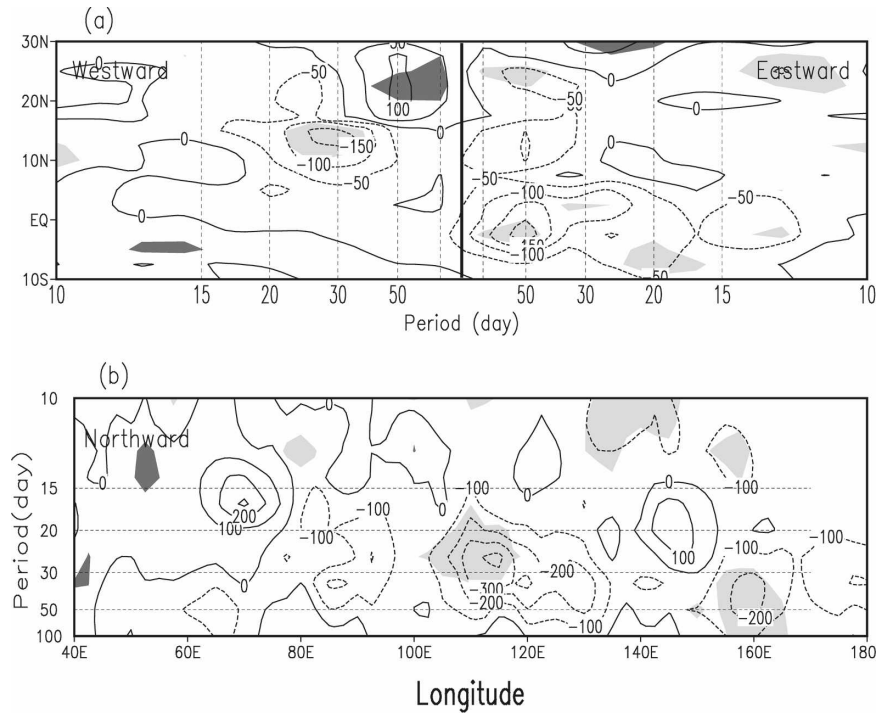


FIG. 14. BISO energy spectrum differences between El Niño and La Niña decaying summers for (a) the zonal wavenumber 1 westward- and eastward-propagating modes and (b) the meridional wavenumber 1 northward-propagating mode. Shading indicates the 95% CL.

Developing of EL Niño, LA Niña, diff. 850hPa

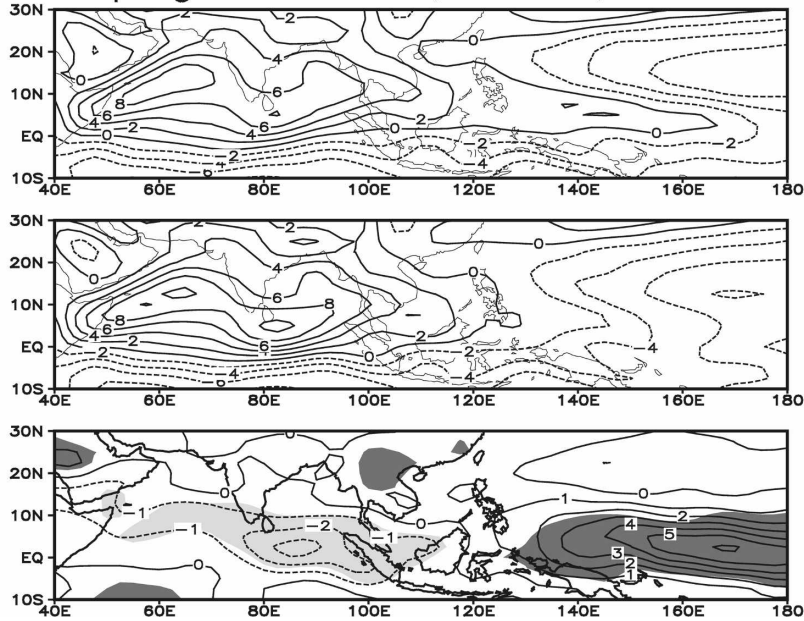


FIG. 15. Composite 850-hPa zonal wind fields ($m s^{-1}$) in the (a) El Niño and (b) La Niña developing summer and (c) their difference. Shading in (c) indicates the 95% CL.

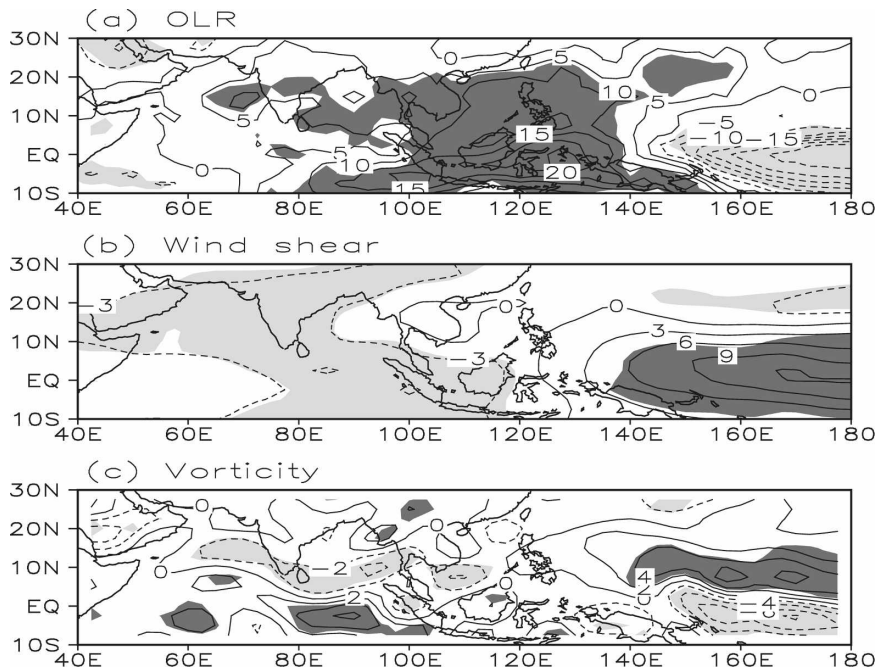


FIG. 16. The difference field of (a) OLR ($W m^{-2}$), (b) vertical zonal wind shear ($u_{850} - u_{200}$; $m s^{-1}$), and (c) 850-hPa vorticity ($10^{-6} s^{-1}$) between El Niño and La Niña developing summer. Shading indicates the 95% confidence level. Negative values in (a) indicate the enhanced convection, whereas positive values in (b) and (c) indicate the increase of the vertical easterly wind shear and vorticity.

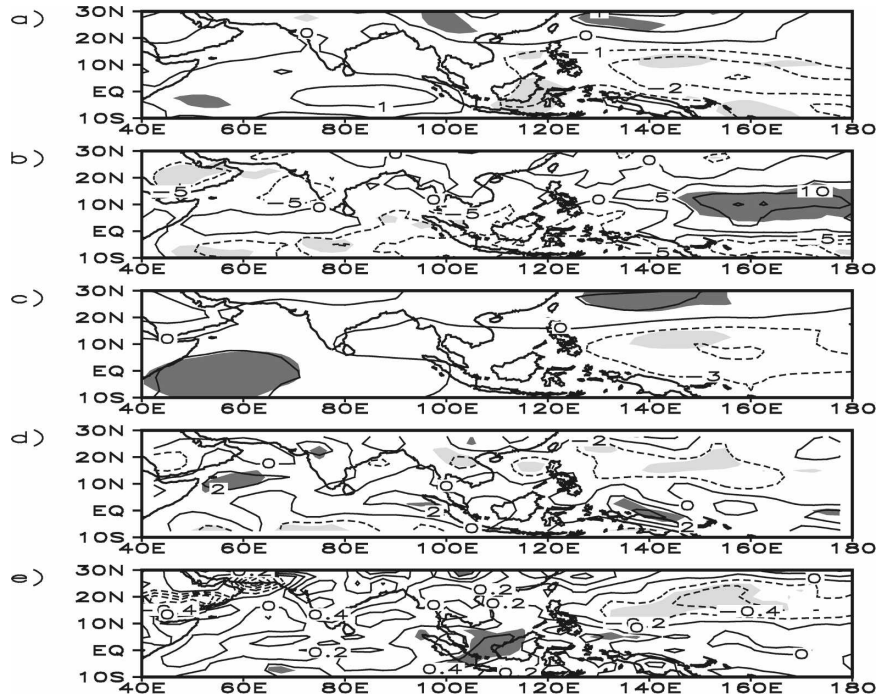


FIG. 17. The difference field of (a) 850-hPa zonal wind (m s^{-1}), (b) OLR (Wm^{-2}), (c) vertical zonal wind shear ($u_{850} - u_{200}$; m s^{-1}), (d) 850-hPa vorticity (10^{-6} s^{-1}), and (e) 925-hPa specific humidity (g kg^{-1}) between El Niño and La Niña decaying summer. Shading indicates the 95% CL.

pine Sea anticyclone anomaly leads to the suppression of the WNP monsoon and thus the decrease of the vertical easterly shear (Fig. 17c), the cyclonic vorticity (Fig. 17d), and the near-surface specific humidity (Fig. 17e) in situ. Such a change in the atmospheric background condition suppresses the Rossby wave development (Wang and Xie 1996). As the westward- and northward-propagating modes over the WNP are closely linked to moist Rossby waves and background horizontal and vertical shear, both the westward and northward BSISO spectrums are suppressed (Fig. 14). Because of the asymmetry of the anomalous circulation pattern (i.e., maximum zonal wind, low-level vorticity, and vertical shear anomalies shift to the southeast quadrant of the tropical WNP during the El Niño developing summer while they shift to the northwest quadrant during the El Niño decaying summer), the amplitude of the northward-propagating ISO energy spectrum also exhibits a distinctive asymmetry between El Niño developing and decaying summers. A similar argument may apply to the asymmetry between the La Niña developing and decaying summers. To sum up, the asymmetric behavior in BSISO propagation and intensity results primarily from the asymmetry of the atmospheric background flow change between the developing and decaying phases of ENSO.

6. Conclusions

The characteristics of the climatological boreal summer (May–October) ISO energy spectrum distribution and its variations during the ENSO developing and decaying phases over the Indo–western Pacific regions were examined using the 25-yr (1979–2003) observational data that include daily OLR and monthly SST, wind, and humidity fields. The main conclusions are stated below.

The BSISO energy in the Indian Ocean–western Pacific region (10°S – 30°N , 40°E – 180°) is confined to the lowest wavenumbers in both zonal and meridional directions and the 30–60-day period, for either propagating or stationary modes. The BSISO energy spectrum distribution exhibits a distinctive regional characteristic. The stationary and eastward-propagating modes are most pronounced at the equator (5°S – 5°N) and become weaker toward higher latitudes. The westward-propagating modes are dominant in the off-equatorial region (10° – 20°N). While the eastward-propagating ISO spectrum agglomerates on the 30–60-day period and zonal wavenumber 1, the westward-propagating mode covers wider spatial (wavenumber) and temporal (period) range. The meridional propagating modes are pronounced over the Indian Ocean, SCS, and western

Pacific, with a maximum energy spectrum over the eastern Indian Ocean and a minimum energy spectrum over Sumatra and Indochina peninsula region (95° – 105° E). While the northward propagation is the dominant mode in the meridional direction for all wavenumbers and periods, more complex features appear in the zonal direction. Along the ABS latitudes, the dominant mode for wavenumber 1 is the eastward propagation at the 30–60-day period, but becomes the westward propagation at the 10–20-day period; for wavenumber 2, the dominant mode is the westward propagation at both the 30–60-day and 10–20-day periods. Compared to the absolute amplitude of both zonal and meridional mode energy spectrum, northward propagation is the most predominant mode in boreal summer over the Indo–western Pacific regions.

The BSISO–ENSO relationship was examined separately in the El Niño and La Niña developing and decaying phases. During boreal summer of the El Niño (La Niña) developing year, the strongest change of BSISO is found in the equatorial region, where both the stationary and eastward-propagating modes are enhanced (weakened). In addition, the northward-propagating mode over the western Pacific (east of 140° E) is also strengthened (weakened) significantly. Over SCS longitudes (105° – 120° E), the northward propagation is weakened (enhanced) at the 30–60-day period but opposite at the 10–20-day period. During the El Niño (La Niña) decaying summer, the eastward-propagating BSISO weakens (strengthens) at the equator, which is opposite to that during the developing summer; the westward-propagating mode off the equator and the northward-propagating mode over SCS and western Pacific are also suppressed (enhanced) distinctly.

The amplitude of the BSISO variation is stronger in the ENSO decaying summer than in the developing summer. For example, the maximum change of energy spectrum of the northward- and westward-propagating BSISO between El Niño and La Niña decaying summers is about 61% and 36% of the climatological values, respectively. The cause of the asymmetry is attributed to the asymmetry of the anomalous circulation pattern; that is, maximum zonal wind, low-level vorticity, and vertical shear anomalies shift to the southeast quadrant of the tropical western North Pacific during the El Niño developing summer, while they shift to the northwest quadrant during the El Niño decaying summer. There is also an asymmetry between El Niño and La Niña during both the developing and decaying phases. The cause of the asymmetry during the same developing or decaying phases is due to the amplitude and pattern asymmetries of El Niño and La Niña and

the nonlinearity of atmospheric responses to SSTA forcing.

The dependence of BSISO behaviors on ENSO phases is due to the distinctive change of the background mean flow during the ENSO developing and decaying summers. In the El Niño developing summer, the westerly wind and large-scale convection are enhanced over the equatorial western and central Pacific. As a result, the equatorial coupled Kelvin–Rossby wave packet may reach the easternmost location. This leads to more Rossby wave emanation from the equatorial wave packet east of 140° E. Meanwhile, the background easterly vertical shear and low-level cyclonic vorticity extend southeastward in the WNP, favoring the growth of Rossby waves. Consequently, the westward- and northward-propagating ISO over the western Pacific (east of 140° E) is enhanced. The conditions are in general reverse in the La Niña developing summer.

In the El Niño decaying summer, the equatorial coupled Kelvin–Rossby wave packet is weakened because of the enhanced equatorial easterly and suppressed convection in the western Pacific. Meanwhile, a low-level anticyclone anomaly appears over the Philippine Sea, which results in the weakening of the local background easterly shear, low-level cyclonic vorticity, and specific humidity. These changes cause the decaying of Rossby waves, and weaken the westward- and northward-propagating BSISO. The conditions are reverse in the La Niña decaying summer.

This study analyzes the observational characteristics of BSISO energy spectrum using daily OLR data. It is unclear how sensitive the BSISO energy distribution is when a different variable other than OLR (e.g., zonal wind, pressure, humidity, or precipitation) or a different analysis method is used. These concerns require further research.

Acknowledgments. The authors thank Dr. Haiyan Teng for providing the wavenumber–frequency analysis code. This research was supported by NSFC Grants 40675055/40628006 and Guangdong Natural Science Foundation under Grant 06020745. TL was also supported by ONR grants N000140710145, N00173061G031, and N000140810256 and by the International Pacific Research Center that is sponsored by the Japan Agency for Marine–Earth Science and Technology (JAMSTEC), NASA (NNX07AG53G), and NOAA (NA17RJ1230).

REFERENCES

- Chen, L., C. Zhu, W. Wang, and P. Zhang, 2001: Analysis of the characteristics of 30–60 day low-frequency oscillation over Asia during 1998 SCSMEX. *Adv. Atmos. Sci.*, **18**, 623–638.

- Chen, T.-C., and M. Murakami, 1988: The 30–50 day variation of convective activity over the western Pacific Ocean with the emphasis on the northwestern region. *Mon. Wea. Rev.*, **116**, 892–906.
- Chen, X., H. Wang, and Q. Zeng, 2000: *Atmospheric Intraseasonal Oscillation and its Interannual Variation*. Beijing China Meteorological Press, 176 pp.
- Fink, A., and E. Speth, 1997: Some potential forcing mechanisms of the year-to-year variability of the tropical convection and its intraseasonal (25–70-day) variability. *Int. J. Climatol.*, **17**, 1513–1534.
- Fu, X., and B. Wang, 2004: The boreal-summer intraseasonal oscillations simulated in a hybrid coupled atmosphere–ocean model. *Mon. Wea. Rev.*, **132**, 2628–2649.
- Gutzler, D. S., 1991: Interannual fluctuations of intraseasonal variance of near-equatorial zonal winds. *J. Geophys. Res.*, **96**, 3173–3185.
- Han, R., W. Li, and M. Dong, 2006: The impact of 30–60 day oscillations over the subtropical Pacific on the East Asian summer rainfall (in Chinese). *Acta Meteor. Sinica*, **64**, 149–163.
- Hayashi, Y., 1982: Space–time spectral analysis and its applications to atmospheric waves. *J. Meteor. Soc. Japan*, **60**, 156–171.
- Hendon, H. H., and M. L. Salby, 1994: The life cycle of Madden–Julian oscillation. *J. Atmos. Sci.*, **51**, 2207–2219.
- , C. Zhang, and J. Glick, 1999: Interannual variation of the Madden–Julian oscillation during austral summer. *J. Climate*, **12**, 2538–2550.
- Jiang, X., T. Li, and B. Wang, 2004: Structures and mechanisms of the northward propagating boreal summer intraseasonal oscillation. *J. Climate*, **17**, 1022–1039.
- Ju, J., C. Qian, and J. Cao, 2005: The intraseasonal oscillation of East Asian summer monsoon (in Chinese). *Chinese J. Atmos. Sci.*, **29**, 187–194.
- Kanamitsu, M., W. Ebisuzaki, J. Woollen, S.-K. Yang, J. J. Hnilo, M. Fiorino, and G. L. Potter, 2002: NCEP–DOE AMIP-II Reanalysis (R-2). *Bull. Amer. Meteor. Soc.*, **83**, 1631–1643.
- Kang, I.-S., and J.-S. Kug, 2002: El Niño and La Niña sea surface temperature anomalies: Asymmetry characteristics associated with their wind stress anomalies. *J. Geophys. Res.*, **107**, 4372, doi:10.1029/2001JD000393.
- Kessler, W. S., 2001: EOF representations of the Madden–Julian oscillation and its connection with ENSO. *J. Climate*, **14**, 3055–3061.
- Krishnamurti, T. N., and D. Subrahmanyam, 1982: The 30–50 day mode at 850 mb during MONEX. *J. Atmos. Sci.*, **39**, 2088–2095.
- Lau, K.-M., and P. H. Chan, 1986: Aspects of the 40–50 day oscillation during the northern summer as inferred from outgoing longwave radiation. *Mon. Wea. Rev.*, **114**, 1354–1367.
- , and S. Yang, 1996: Seasonal variation, abrupt transition and intraseasonal variability associated with the Asian summer monsoon in the GLA GCM. *J. Climate*, **9**, 965–985.
- Li, C., and G. Li, 1997: Evolution of intraseasonal oscillation over the tropical western Pacific/South China Sea and its effect to the summer precipitation in Southern China. *Adv. Atmos. Sci.*, **14**, 246–254.
- , and J. Wu, 2000: On the onset of the South China Sea summer monsoon in 1998. *Adv. Atmos. Sci.*, **17**, 193–204.
- , Z. Long, and Q. Zhang, 2001: Strong/weak summer monsoon activity over the South China Sea and atmospheric intraseasonal oscillation. *Adv. Atmos. Sci.*, **18**, 1146–1160.
- , —, and M. Mu, 2003: Atmospheric intraseasonal oscillation and its important effect (in Chinese). *Chin. J. Atmos. Sci.*, **27**, 518–535.
- , X. Jia, and M. Dong, 2006: The importance of the atmospheric intraseasonal oscillation in the prediction of the weather and climate (in Chinese). *Acta Meteor. Sinica*, **64**, 412–419.
- Li, T., and B. Wang, 1994: The influence of sea surface temperature on the tropical intraseasonal oscillation: A numerical experiment. *Mon. Wea. Rev.*, **122**, 2349–2362.
- Liang, J., A. Lin, and C. Li, 2005: ISOs of TBB over SCS and vicinity as well as its relationship with ENSO (in Chinese). *Acta Meteor. Sinica*, **63**, 267–277.
- Liebmann, B., and C. A. Smith, 1996: Description of a complete (interpolated) outgoing longwave radiation dataset. *Bull. Amer. Meteor. Soc.*, **77**, 1275–1277.
- Lin, A., 1998: The characteristics of low-frequency oscillation over South China Sea. *J. Trop. Meteor.*, **4**, 141–147.
- , Q. Wan, J. Liang, and J. Yuan, 2004: Influence of tropical southwest monsoon on tropical cyclone Vongfong (0214) (in Chinese). *Acta Meteor. Sinica*, **62**, 841–850.
- , J. Liang, and C. Li, 2006: Characteristics of frequency spectrum variation of intraseasonal oscillation of convection during South China Sea summer monsoon. *J. Trop. Meteor.*, **12**, 34–40.
- , —, —, D. Gu, and B. Zheng, 2007: Monsoon circulation background of ‘0506’ continuous rainstorm in South China (in Chinese). *Adv. Water Sci.*, **18**, 424–432.
- Long, Z., and C. Li, 2002: Interannual variations of tropical atmospheric 30–60 day low-frequency oscillation and ENSO cycle. *Chin. J. Atmos. Sci.*, **26**, 51–62.
- Madden, R. A., and P. R. Julian, 1971: Detection of a 40–50 day oscillation in the zonal wind in the tropical Pacific. *J. Atmos. Sci.*, **28**, 702–708.
- , and —, 1994: Observation of the 40–50-day tropical oscillation: A review. *Mon. Wea. Rev.*, **122**, 814–837.
- Mao, J., and G. Wu, 2005: Intraseasonal variability in the Yangtze–Huaihe river rainfall and subtropical high during the 1991 meiyu period (in Chinese). *Acta Meteor. Sinica*, **63**, 762–770.
- Mu, M., and C. Li, 2000: On the outbreak of the South China Sea summer monsoon in 1998 and activity of atmospheric intraseasonal oscillation (in Chinese). *Climate Environ. Res.*, **5**, 375–387.
- Rayner, N. A., E. B. Horton, D. E. Parker, C. K. Folland, and R. B. Hackett, 1996: Version 2.2 of the global sea-ice and sea surface temperature data set, 1903–1994. Climate Research Tech. Note 74, Hadley Centre for Climate Prediction and Research, Met Office, 43 pp.
- Salby, M. L., and H. H. Hendon, 1994: Intraseasonal behavior of clouds, temperature and motion in the tropics. *J. Atmos. Sci.*, **51**, 2220–2237.
- Shi, X., and Y. Ding, 2000: A study on extensive heavy rain processes in south China and the summer monsoon activity in 1994 (in Chinese). *Acta Meteor. Sinica*, **58**, 666–678.
- Teng, H., and B. Wang, 2003: Interannual variations of the boreal summer intraseasonal oscillation in the Asian–Pacific region. *J. Climate*, **16**, 3571–3584.
- Waliser, D. E., 1996: Formation and limiting mechanisms for very high sea surface temperature: Linking the dynamics and the thermodynamics. *J. Climate*, **9**, 161–188.

- Wang, B., and H. Rui, 1990: Synoptic climatology of transient tropical intraseasonal convection anomalies: 1975–1985. *Meteor. Atmos. Phys.*, **44**, 43–61.
- , and X. Xie, 1996: Low-frequency equatorial waves in vertically sheared zonal flow. Part I: Stable waves. *J. Atmos. Sci.*, **53**, 449–467.
- , and —, 1997: A model for the boreal summer intraseasonal oscillation. *J. Atmos. Sci.*, **54**, 72–86.
- , and X. Xu, 1997: Northern Hemisphere summer monsoon singularities and climatological intraseasonal oscillation. *J. Climate*, **10**, 1071–1085.
- , and LinHo, 2002: Rainy season of the Asian–Pacific summer monsoon. *J. Climate*, **15**, 386–398.
- , R. Wu, and X. Fu, 2000: Pacific–East Asian teleconnection: How does ENSO affect East Asian climate? *J. Climate*, **13**, 1517–1536.
- Wheeler, M., and G. N. Kiladis, 1999: Convectively coupled equatorial waves: Analysis of clouds and temperature in the wavenumber–frequency domain. *J. Atmos. Sci.*, **56**, 374–399.
- Xu, G., Q. Zhu, J. Xue, and J. He, 2004: A pilot study of propagation mechanisms of precipitation low-frequency variation over China in 1998 (in Chinese). *Chin. J. Atmos. Sci.*, **28**, 736–746.
- Yang, H., and C. Li, 2003: The relation between atmospheric intraseasonal oscillation and summer severe flood and drought in Changjiang-Huaihe river basin. *Adv. Atmos. Sci.*, **20**, 540–553.
- , and —, 2005: A study of propagation of tropical intraseasonal oscillation and its influence mechanism (in Chinese). *Climate Environ. Res.*, **10**, 145–156.
- Yasunari, T., 1979: Cloudiness fluctuations associated with the Northern Hemisphere summer monsoon. *J. Meteor. Soc. Japan*, **57**, 227–242.
- Zhang, Y., T. Li, B. Wang, and G. Wu, 2002: Onset of the summer monsoon over the Indochina Peninsula: Climatology and interannual variations. *J. Climate*, **15**, 3206–3221.
- Zhu, B., and B. Wang, 1993: The 30–60 day convection seesaw between the tropical Indian and western Pacific Oceans. *J. Atmos. Sci.*, **50**, 184–199.
- Zhu, C., T. Nakazawa, and J. Li, 2004: Modulation of tropical depression/cyclone over the Indian–western pacific oceans by Madden–Julian oscillation (in Chinese). *Acta Meteor. Sinica*, **62**, 42–50.

Copyright of *Journal of Climate* is the property of *American Meteorological Society* and its content may not be copied or emailed to multiple sites or posted to a listserv without the copyright holder's express written permission. However, users may print, download, or email articles for individual use.